

This is the accepted manuscript made available via CHORUS. The article has been published as:

Oxidation and reduction of Pd(100) and aerosol-deposited Pd nanoparticles

R. Westerström, M. E. Messing, S. Blomberg, A. Hellman, H. Grönbeck, J. Gustafson, N. M. Martin, O. Balmes, R. van Rijn, J. N. Andersen, K. Deppert, H. Bluhm, Z. Liu, M. E. Grass, M. Hävecker, and E. Lundgren

Phys. Rev. B **83**, 115440 — Published 23 March 2011

DOI: [10.1103/PhysRevB.83.115440](https://doi.org/10.1103/PhysRevB.83.115440)

The oxidation and reduction of Pd(100) and aerosol deposited Pd nanoparticles

R. Westerström¹, M. E. Messing², S. Blomberg¹, A. Hellman³, H. Grönbeck³, J. Gustafson¹, N. M. Martin¹, O. Balmes⁴, R. van Rijn^{4,5}, J. N. Andersen¹, K. Deppert², H. Bluhm⁶, Z. Liu⁶, M. E. Grass⁶, M. Hävecker⁷, and E. Lundgren¹

¹*Department of Synchrotron Radiation Research,
Lund University, Box 118, SE-221 00, Sweden*

²*Solid State Physics, Lund University,
Box 118, S-221 00 Lund, Sweden*

³*Competence Center for Catalysis and Department of Applied Physics,
Chalmers University of Technology,
SE-412 96 Göteborg, Sweden*

⁴*ESRF, B. P. 220, F-38043 Grenoble, France*

⁵*Kamerlingh Onnes Laboratory,
Leiden University, P.O. Box 9504,
2300 RA Leiden, The Netherlands*

⁶*ALS, Lawrence Berkeley National Laboratory,
Berkeley, CA 94720, USA*

⁷*Fritz Haber Institute of the Max Planck Society Department
of Inorganic Chemistry Faradayweg 4-6 D - 14195 Berlin*

Using *in situ* high pressure X-ray photoelectron spectroscopy (HPXPS), we have followed the oxidation and the reduction of Pd model catalysts in oxygen and CO pressures in the mbar range. The study includes a Pd(100) single crystal as well as SiO_x supported Pd nanoparticles of 15 or 35 nm diameter respectively. We demonstrate that also nanoparticles form ultra-thin surface oxides prior to the onset of the bulk PdO. The Pd nano particles are observed to bulk oxidize at sample temperatures 40 degrees lower than the single crystal surface. In the Pd 3d_{5/2} and the O 1s spectrum we identify a component corresponding to under-coordinated atoms at the surface of the PdO oxide. The experimentally observed PdO CLS is supported by density functional theory calculations (DFT). In a CO atmosphere, the Pd 3d_{5/2} component corresponding to under-coordinated PdO atoms is shifted by +0.55 eV with respect to PdO bulk, demonstrating that CO molecules preferably adsorbs at these sites. CO coordinated to Pd atoms in the metallic and the oxidized phase can also be distinguished in the C 1s spectrum. The initial reduction by CO is similar for the single crystal and the nanoparticle samples, but after the complete removal of the oxide we detect a significant deviation between the two systems, namely that the nanoparticles incorporate carbon to form a Pd carbide. Our results indicates that CO can dissociate on the nanoparticle samples, whereas no such behavior is observed for the Pd(100) single crystal. These results demonstrate the similarities, as well as the important differences, between the single crystal used as model systems for catalysis and nm sized particles on oxide supports.

PACS numbers: 68.47.Gh, 79.60.-i, 81.16.Pr

I. INTRODUCTION

Motivated mainly by the relevance for oxidation and reduction catalysis, the interaction between oxygen and single crystal surfaces of transition metals has been studied in great detail in recent years. These studies have generally been performed under UHV compatible conditions, where it is possible to have a very good control of the abundance of molecules on the surface. Such studies have led to a thorough understanding of the adsorption and dissociation of O₂ on metals such as Rh, Pt and Pd that are e.g. used as the active part in car exhaust catalytic converters.

Recently, however, there has been a strong effort on studying more relevant model systems for catalysis, and several groups aim at doing surface science studies under higher pressures and more complex surfaces such as oxide

supported nanoparticles.

By studying the interaction between single crystals and oxygen under higher O₂ exposures, a new family of ultra-thin oxide structures — so-called surface oxides — has been found to form prior to the onset of the bulk oxidation [1]. For Pd(100) and Pd(111), the surface oxides have been thoroughly characterized in previous studies [2–5]. In the case of Pd(110), no surface oxide has been found so far [6, 7]. In parallel, it has been reported that oxidation of CO to CO₂ over transition metal surfaces, is often more efficient on surfaces with a thin oxide (such as a surface oxide) than on the corresponding metallic surface [8–22]. Furthermore, in a recent theoretical paper [23], Rogal *et al.* suggest that the surface oxide is indeed the most active phase for CO oxidation under conditions representative of technological catalysis. Although these results are still under debate [24, 25] it is clearly of major

relevance to study the oxidation of such surfaces under catalytically relevant pressures.

Much less is known on the oxidation of Pd particles, and the role of Pd oxides formed on Pd nanoparticles during catalytic oxidation reactions under realistic conditions. One step towards an increased understanding is to study the oxygen interaction with Pd particles and the oxide formation. Under UHV conditions, such studies have been performed previously. Shaikhutdinov *et al.* [26] studied the interaction between oxygen and Pd particles on a thin alumina film grown on a NiAl(110) substrate, and found that oxygen dissociates on the Pd particles, migrates through the Alumina film and reacts with the metallic NiAl substrate underneath, and thereby increasing the thickness of the Alumina film until a temperature dependent self-limited thickness of the film is reached, and atomic oxygen start to adsorb on the particles. Under these conditions, no Pd oxide was formed, and adsorption-desorption properties were found to be similar to those of Pd(111). Another set of studies have been performed on Pd particles grown on an Fe₃O₄ film on Pt(111) [27–29]. Molecular beam studies suggests that the oxidation of these particles starts at the interface between the Pd particle and the Fe₃O₄ film and that the oxygen uptake into the Pd particles increases for Pd particles below 20 nm with a maximum at approximately 7 nm.

Since the majority of traditional surface characterization tools use electrons as a probe in order to enhance the surface sensitivity, most studies of high pressure structures have been done *ex situ* in UHV after quenching the structure by cooling. It is, however, difficult to know if the structure is the same before and after this quenching process, and especially for catalytically active structures, formed in the presence of more than a single gas, this is often not the case. In order to follow processes as they occur, *in situ* measurements are required. Until recently, such studies has been limited to surface X-ray diffraction, which requires epitaxial structures, STM, which requires flat surfaces, and different kinds of infra-red spectroscopy methods that are limited to characterizing the molecules found on the surface. Recently, however, a few experimental systems have been developed that, by the use of differential pumping and strong focusing of the emitted electrons, allowing for X-ray photoelectron spectroscopy to be used under pressures up to 10 mbar, so-called High Pressure X-ray Photoelectron Spectroscopy (HPXPS) [30, 31].

In this paper we report an *in situ* high pressure X-ray photoelectron spectroscopy study of the oxidation process as well as the reduction with CO of Pd(100) and size selected aerosol deposited [32] Pd nanoparticles on SiO_x. Nanoparticles with a diameter of 15 and 35 nm were studied, but no significant difference in oxidation and reduction behavior between the two particle sizes could be observed. The oxidation process is also similar to that of the Pd(100) single crystal surface, with the formation of a thin surface oxide prior to the bulk

oxidation. The most pronounced difference is an approximately 40 degree lower bulk oxidation temperature of the particles as compared to the single crystal, when using 0.5 mbar of O₂ and increasing the temperature. Both for particles and single crystal we identify a surface core level shift (SCLS) for the Pd bulk oxide (PdO) surface. The identified Pd surface atoms in the PdO are shown to be affected when the PdO is exposed to 0.5 mbar of CO at 100-120°C, indicating that CO adsorbs on the PdO under these conditions. Simultaneously, a component in the C1s region can be identified as CO adsorbing on the PdO. During the reduction with CO, more significant differences between the single crystal and the particles can be observed. We can confirm recent results indicating the formation of a Pd carbide [33] on the Pd nanoparticles which does not occur in the single crystal case.

II. EXPERIMENTAL

The preparation of the nanoparticle samples are described in detail in Ref. [34]. In brief, aerosol Pd particles were size selected and deposited onto a Si wafer that has been cleaned by HF etching and brought out in air in order to grow a native SiO_x oxide. Two kinds of nanoparticle samples were used, with particle diameters of 15 and 35 nm, respectively. As reported in Ref. [34], the resulting samples are highly carbon contaminated and the Pd nanoparticles are covered by a shell of Pd carbide. This contamination can be removed through oxidation. To remove the oxide this was followed by a reduction cycle in CO, which resulted in the return of the carbide shell. Therefore, for the nanoparticle samples, the oxidation process reported below starts from particles with a carbide shell rather than pure Pd particles. The nanoparticle samples were transported to the different experimental locations in air.

The single crystal Pd(100) surface was cleaned by cycles of Ar⁺ sputtering and subsequent anneals, and by keeping the crystal in 10⁻⁷ mbar O₂ while annealing between 100 to 700°C, followed by a flash in vacuum in order to remove residual O. After the cleaning procedure no contaminants such as carbon could be detected.

X-Ray Photoelectron Spectroscopy measurements were performed at the Molecular Science beamline 11.0.2 at the Advanced Light Source (ALS) in Berkeley, USA, using a photon energy of 525 eV and at the ISSS endstation at BESSY in Berlin, Germany. The photon energy was kept constant throughout the experiment, and calibrated from the fermi level of the non-oxidized single crystal and Pd nanoparticles. Since the particles in this study are relatively large (> 15 nm), we do not expect to observe a size induced shift of i.e. the Pd bulk component as compared to the single crystal. Furthermore, we do not observe a shift of the spectrums as the samples where oxidized, indicating that the sample remains conducting.

The Pd(100) spectrum recorded before the oxidation

cycle is decomposed using a single component, although a surface component would be expected [35]. The reasons for the absence of a surface component could be possible hydrogen contamination, which would shift the surface component underneath the bulk component.

III. COMPUTATIONAL METHOD

The density functional theory (DFT) was employed using an implementation with plane-waves and pseudo-potentials [36, 37]. The spin polarized Perdew-Burke-Ernzerhof (PBE) approximation was used for the exchange and correlation (xc) functional [38] and ultrasoft scalar-relativistic pseudo potentials were used to describe the interaction between the valence electrons and the core [39]. The number of electrons treated variationally for each element were: Pd(10), O(6) and C(4). A plane-wave kinetic energy cut-off of 28 Ry was used to expand the Kohn-Sham orbitals.

The lattice constant for Pd (cubic - fcc) is calculated to be 3.93 Å. The corresponding values for PdO (tetragonal) are 3.11 and 5.45 Å. The results are within 2 percent of the experimental lattice constants. The heat of formation for PdO with respect to Pd and O₂ in the gas phase is calculated to be 0.95 eV, which is close to the experimental value of 0.97 eV [40].

The bare Pd(100) surface was represented by five atomic layers in a $p(2 \times 2)$ surface cell. The bare Pd(100) surface was represented by a $p(2 \times 2)$ surface cell and five atomic layers. To model the Pd(100)- $\sqrt{5}$ R27° surface oxide (hereafter denoted $\sqrt{5}$), the oxide monolayer was supported on a five layer Pd(100) slab. Two oxide surfaces were considered, namely PdO(100) and PdO(101). PdO(100) which is the most stable surface oxide termination [41] has all Pd atoms coordinated to four O atoms. PdO(101), which is included because the $\sqrt{5}$ -structure is based on this structure, has in each surface cell two two-fold coordinated and two four-fold coordinated Pd atoms. PdO(100) was modeled by six bi-layers, whereas six tri-layers was used for PdO(101). Repeated slabs are separated by at least 12 Å vacuum. Reciprocal space integration over the Brillouin zone is approximated with a finite sampling of 8 special k-points for Pd(100), $\sqrt{5}$ and PdO(101), whereas 10 k-points were used for PdO(100). Structural optimization was performed without any constraints. For all systems, the bond lengths around a Pd atom in the center of the slab are within 0.2 % of the corresponding bulk values. The surface core level shifts (SCLS) for C(1s), O(1s) and Pd(3d) were evaluated by the use of pseudo-potentials that were generated with an electron hole in respective shell. A Pd(3d) core hole in the center of the slab was used to model the bulk reference. The approach assumes complete screening of the core-hole and has been used successfully over the years [42].

IV. EXPERIMENTAL RESULTS

A. *In situ* oxidation of Pd(100) and Pd particles

Fig. 1 shows *in situ* HPXPS results following the Pd $3d_{5/2}$ level during the oxidation process of Pd(100) and 15 nm Pd nanoparticles in 0.5 mbar of oxygen and step-wise increasing sample temperature. Starting with the Pd(100) data in Fig. 1a, we recognize the spectrum found at 70°C as corresponding to a mixture between the $c(2 \times 2)$ and (5×5) low oxygen coverage structures [2]. The spectrum can be decomposed using three components corresponding to the bulk of the crystal (grey), the clean surface (brown) and one broad component corresponding to Pd atoms coordinated to one or two O atoms (black). Upon further heating this structure evolves into the $\sqrt{5}$ surface oxide structure [2], recognized mainly from the two components shifted towards higher binding energies and corresponding to Pd atoms within the surface oxide that are coordinated to two and four O atoms respectively, see model I and II in Fig. 1. At 150°C this transition is complete, and the characteristic peaks are found at chemical shifts of +0.38 and +1.3 eV relative to the bulk peak, in good agreement with previously reported data [2].

At temperatures above 200°C, a new component at +1.6 eV relative to the bulk Pd appears in the spectra. We attribute this peak to bulk PdO [43]. When we reach a sample temperature of 270°C the oxidation process has progressed to such an extent that the bulk Pd metal is not detectable using XPS. Note, however, that the peak at +1.3 eV still remains in the spectrum together with the bulk PdO component at +1.6 eV. We interpret this as under-coordinated atoms at the surface of the PdO film exhibiting a surface core level shift of -0.3 relative to the bulk PdO, which will be further supported by the *ab initio* calculations and CO adsorption data below. The use of two components to decompose the PdO is different from previous oxidation studies using Pd(111) to form the PdO [44–46].

Additional support for the use of a surface component when decomposing the Pd $3d_{5/2}$ and the O1s levels from PdO is presented in Fig. 2. In this figure we have studied the energy dependence of the different components in the O 1s and the Pd $3d_{5/2}$ regions, in order to probe the presence of surface related electron emission. Starting with the O 1s shown in Fig. 2 (a), we find two components, one at approximately 528.5 eV and one at 529.8 eV corresponding to a shift of approximately +1.3 eV. The energy dependent measurements show that the high binding energy component originates from O atoms deeper in the sample while the low binding energy component is from O at the surface of the PdO film. Thus, the surface core level shift in the O 1s is approximately -1.3 eV with respect to the 1s binding energy of bulk O in PdO. The reason that the Pd 3p component is difficult to observe in the O 1s 625 eV spectra is that the cross section for the Pd 3p is much lower than the O 1s at this energy

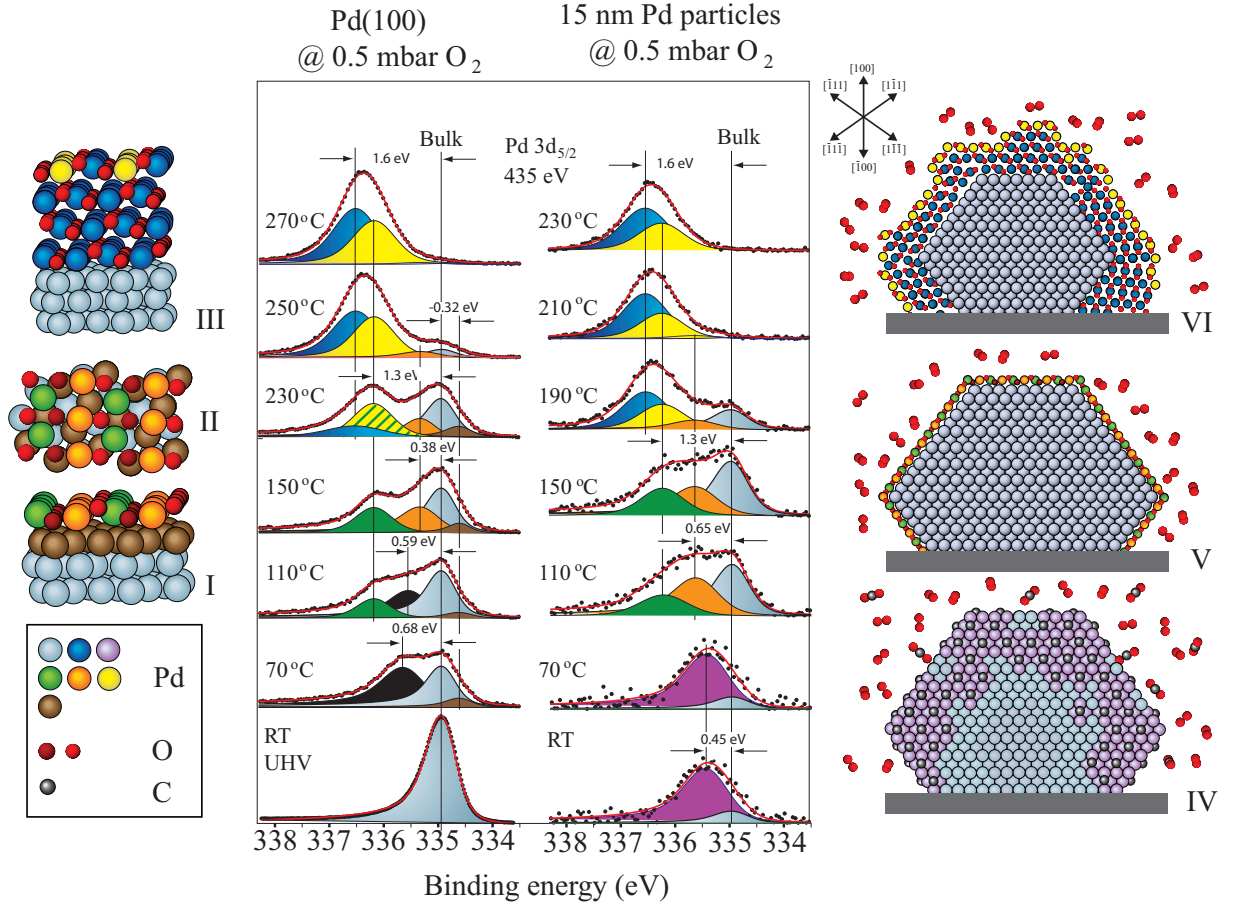


FIG. 1: The oxidation of Pd at 1 mbar O_2 with increasing temperature as probed by the Pd $3d_{5/2}$ level for a Pd(100) single crystal and 15 nm Pd nanoparticles deposited on SiO_x . The models (I)-(III) and (IV)-(VI) illustrates the origin of the different components in the Pd $3d_{5/2}$ spectrum from the Pd(100) single crystal and the 15 nm Pd nanoparticles respectively. (I)-(II) side and top-view of the $\sqrt{5}$ surface oxide. (III) The PdO bulk oxide, which is here orientated so that the PdO[101] direction is parallel to the surface normal of the Pd(100) surface [47]. The component at +1.3 eV is here attributed to 2-folded Pd atoms at the surface (yellow), see section V. (IV)-(VI) Models the nanoparticles displaying a cross section parallel to the (110) plane. These models are only meant as an illustration of the different components in the Pd $3d_{5/2}$ spectrum. For clarity, the models are therefore depicting particles with low index facets and a size smaller than 15 nm. Further, no expected shape changes due to surface compound formation are included. (IV) Pd nanoparticles where the outmost atomic layers consists of a Pd-carbide. (V) A Pd nanoparticle which is covered with different surface oxides. It is here assumed that the $\{100\}$ -facets forms the $\sqrt{5}$ surface oxide, while the $\{111\}$ -facets are covered with a surface oxide similar to the $(\sqrt{6} \times \sqrt{6})$ oxide film [4]. (VI) Pd nanoparticle with a PdO(101) orientation. Since the orientation of the PdO can not be determined by XPS, each facet is here assumed to have a PdO(101) orientation.

as compared to at higher energies. The corresponding measurements for the $3d_{5/2}$ level is shown in Fig. 2 b. In this case, the energy dependence clearly shows that the component shifted by +1.3 eV from the bulk Pd is due to electron emission from Pd atoms at the surface while the +1.6 component is from Pd atoms in the bulk of the PdO surface. Thus, we find a surface core level shift of -0.3 eV for the $3d_{5/2}$ level from PdO on Pd(100).

Returning to Fig. 1, the oxidation data from the nanoparticle sample shown in Fig. 1 are essentially identical to the single crystal, with two exceptions. As mentioned above, it was not possible to produce pure Pd particles, but the particles were always found in either

an oxide or a carbide phase. Hence the oxidation starts from a Pd carbide instead of clean Pd. The second difference is the temperature needed to form the PdO.

At a sample temperature of 150°C, the $3d_{5/2}$ level exhibits a component with a CLS of +1.3 eV, which is characteristic for Pd atoms coordinated to 4 O-atoms. All surface oxides found in previous studies of closed packed and vicinal Pd surfaces have Pd atoms coordinated to 4 O-atoms with a CLS of +1.3 eV [2, 4, 48]. As in the case of the single crystal, it is likely that also the nanoparticles are covered with a surface oxide under these conditions. The onset of the bulk oxide growth, however, is found to be approximately 40°C lower for the nanoparticles, since

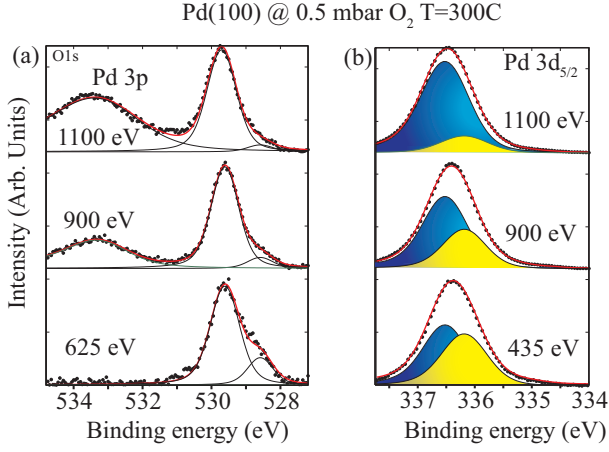


FIG. 2: The energy dependence from PdO formed at Pd(100) for (a) the O 1s level (b) the Pd $3d_{5/2}$.

the bulk signal of the Pd metal is not detectable already at a temperature of 210-230°C. It should be noted that also in the case of Pd particles, we have to use two components to decompose the spectra from a thicker PdO film.

In Fig. 3 we compare the oxidation rate between the 15 and 35 nm Pd particles at 1 mbar of O_2 . The figure shows that there is, within the error margins of the experiment, no difference in the oxidation behavior between nanoparticles of 15 and 35 nm diameter. It also shows that changing the O_2 pressure from 0.5 mbar to 1 mbar does not affect the oxidation rate significantly.

B. *In situ* reduction of Pd(100) and Pd particles

The oxidized samples can now be reduced by CO exposure. In order to follow the reduction within the timescale to record a spectra, we cool the sample to an appropriate reduction temperature before pumping out the O_2 and introducing CO. Fig. 4 shows the Pd $3d_{5/2}$ spectra from an oxidized Pd(100) crystal, just before and right after the introduction of 0.5 mbar CO at 120°C. As the sample is exposed to CO, the PdO surface component is clearly shifted towards higher binding energies, which is understood by CO bonding to the 2-fold coordinated PdO surface atoms. This observation strongly support our deconvolution using two components of the clean PdO $3d_{5/2}$ spectra as discussed above. The spectra also show that the reduction process has started already at this low temperature, but not to the extent that the effect on the intensity of the oxide related peaks is significant.

The complete reduction process for a similarly oxidized Pd(100) sample can be followed in Fig. 5(a). The bottom spectrum is recorded after evacuating the O_2 atmosphere, just before introducing 0.1 mbar CO at around 120°C. As the reduction process proceeds with time, the oxide

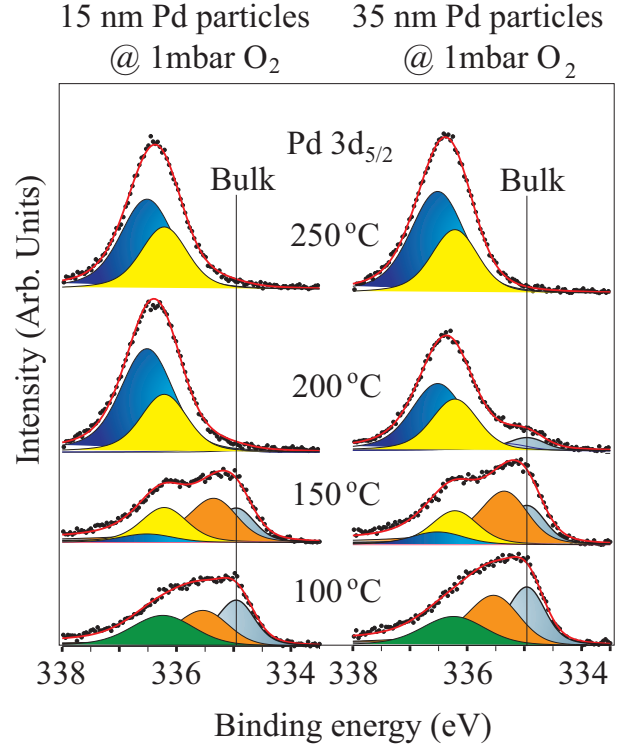


FIG. 3: The oxidation of 15 and 35 nm Pd particles shows no detectable differences. The different components are labeled according to the colors in the models in Fig. 1

related peaks in the Pd $3d_{5/2}$ region decrease in intensity while the components corresponding to metallic bulk Pd and Pd at the surface coordinated to CO adsorbed in bridge sites in agreement with previous studies [49] are increasing.

In order to fit the Pd $3d_{5/2}$ spectra recorded during the reduction process, we have to include an extra component at a binding energy of about 336 eV. We attribute this component to partly reduced Pd atoms, which depending on the coordination of each atom to O and CO are expected to exhibit a range of binding energies between the metallic surface atoms with adsorbed CO found at 335.5 eV (+0.6 eV) and the oxide surface with CO at 336.75 eV. Hence the decompositions of the intermediate stages are not to be considered conclusive, but rather approximative.

In the C 1s spectra we again find several components attributed to CO in different positions. The peak at 285.7 eV is recognized as corresponding to CO adsorbed in bridge sites on the metallic surface [49]. At around 287 eV we find a broad peak which we attribute to CO adsorbed on the oxide. The broad appearance of this peak indicate a mixture of adsorption sites, which will be confirmed by DFT calculations below. Finally, a peak at around 290 eV is found corresponding to CO in gas phase. The gas phase binding energy changes slightly through the reduction process, due to changes in the work

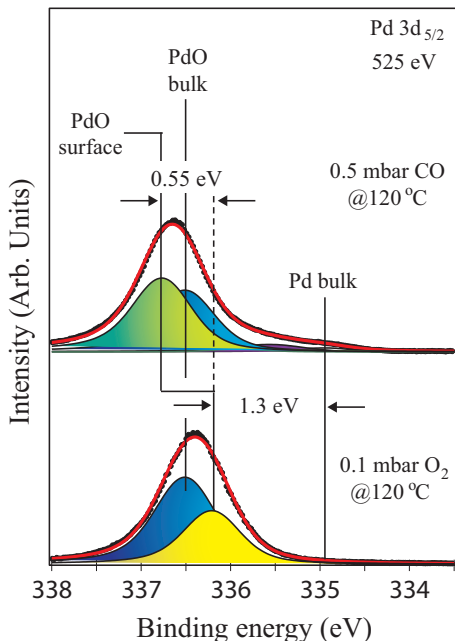


FIG. 4: HPXPS spectra from the $3d_{5/2}$ region of PdO before and after introducing CO. The yellow component corresponds to 2-fold coordinated Pd atoms at the surface of the PdO oxide. As CO is introduced, the PdO-surface component shifts toward higher binding energy. We therefore attribute the shifted component at 336.75 eV (green) to 2-fold coordinated PdO surface atoms bonding with CO.

function. The oxidation-reduction cycle for the Pd(100) crystal is summarized in Fig. 6.

Fig. 5b shows Pd $3d$ spectra from a similar reduction series using 120°C and 0.1 mbar CO for a sample with 15 nm Pd nanoparticles on SiO_x . During the reduction, the differences between the behavior of the nanoparticles and the single crystal are small. The CO induced surface core level shift on the oxide is the same, and the Pd bulk grows slowly together with the peak corresponding to Pd coordinated to adsorbed CO. Once the reduction is complete, however, the spectrum continues to change, and the components corresponding to metallic Pd in the bulk and coordinated to adsorbed CO are replaced by a single component in-between. We attribute this component to the formation of Pd carbide. Of course, some of the intensity of this component could also be from CO adsorbed on the Pd carbide. The experimental binding energy agrees well with calculated Pd $3d$ binding energies for a Pd_6C phase [50]. The reason for not showing the C $1s$ region in the case of the Pd particles is that no C $1s$ intensities can be observed. The reason is the very low carbon coverage (<1.5 % for full Pd_6C formation in the particles) and the three times lower cross section for C $1s$ than Pd $3d$ at these energies. Fig. 7 summarizes the oxidation-reduction cycle of the Pd nanoparticles.

V. CALCULATED CORE LEVEL SHIFTS

The Pd($3d$) SCLS for the bare Pd(100) surface and the $\sqrt{5}$ structure are reported in Table 1. The atoms in the surface layers of Pd(100) experience a shift of -0.36 eV with respect to the bulk reference which is close to the experimental value of -0.40 eV. The Pd atoms in the $\sqrt{5}$ surface oxide are oxidized and have positive shifts with respect to the bulk component. The $3d$ binding energy of the Pd atoms that are two-fold coordinated to oxygen are shifted by +0.34 and +0.45 eV, whereas the four-fold coordinated atoms are shifted by +1.17 and +1.21 eV, respectively. The results are in good agreement with the experiments as well as previous calculations [3]. As a model for a further oxidized Pd(100) surface we have (following Ref. [47]) considered the $\sqrt{5}$ structure with four Pd(101) monolayers. With respect to the monolayer, the components for the two-fold atoms are slightly increased, whereas the components of the four-fold atoms have a minor shift to lower binding energies.

TABLE I: Pd($3d$) SCLS (eV) for Pd(100) and $\sqrt{5}$ with one and four monolayers. S0 denotes a surface atom at the bare Pd(100) surface. For the $\sqrt{5}$ systems, this value is calculated for the backside of the slab. $2f_1$, $2f_2$, $4f_1$ and $4f_2$ denote the four different Pd atoms in the surface layers of the Pd-supported oxide film, see Fig. 8

	S0	$2f_1$	$2f_2$	$4f_1$	$4f_2$
Pd(100)	-0.36				
$\sqrt{5}$ 1ML	-0.35	0.34	0.45	1.17	1.21
$\sqrt{5}$ 4ML	-0.36	0.53	0.53	1.14	1.14

For the clean PdO(101) surface we calculate a shift for Pd($3d$) of -0.55 eV and -0.02 with respect to Pd in the bulk of PdO. The large shift is experienced by the two-fold coordinated atoms. For PdO(100), the Pd surface atoms have shifts in the $3d$ component of only -0.10 eV. The result for the PdO(101) surface can be compared to the 4 ML surface oxide. The Pd atoms in the interior of the film (which all are four-fold coordinated) have an average shift with respect to bulk-Pd of +1.08 eV. Thus, the two-fold coordinated atoms at the surface are shifted by -0.55 eV with respect to this value, in perfect agreement with the PdO(101) bulk calculation. The calculations suggest that a bulk character of the film has evolved already for 4 ML PdO(101) supported on Pd(100).

There are two types of O atoms at the PdO(101) surface: three-fold coordinated and four-fold-coordinated, see Fig. 8. The shifts for the O($1s$) binding energy with respect to O in the bulk of PdO are calculated to be -0.31 and -0.95 eV respectively.

CO adsorption was explored on Pd(100), PdO(101) and 1ML and 4 ML surface oxide films. The energetics of CO adsorption have been investigated previously for the surface oxide films [47, 51, 52]. The present results are in full agreement with the literature. At a coverage

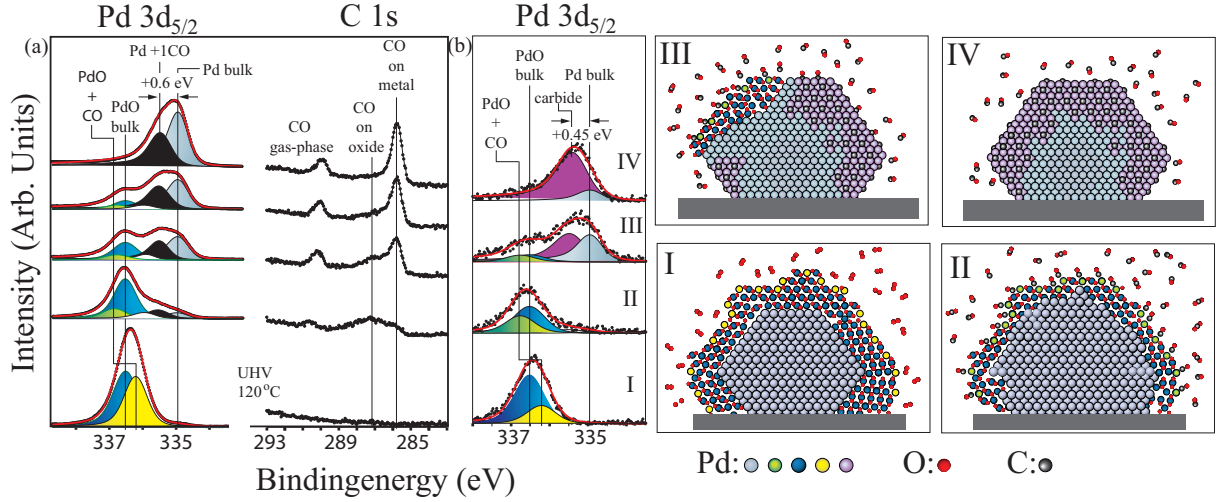


FIG. 5: The CO induced reduction using 0.1 mbar of CO and 120 °C of fully oxidized (a) Pd(100) single crystal. (b) 15 nm Pd particles. (a) The blue, yellow, and green component in the 3d_{5/2} spectrum, corresponds to PdO bulk, 2-fold coordinated PdO surface atoms, and 2-fold coordinated PdO surface atoms bonding with CO, see Fig. 4. The black component originates from Pd atoms on the reduced (100) surface coordinated to 1 CO atom, whereas the white component corresponds to partially reduced Pd atoms coordinated to CO. As CO is introduced the C 1s region exhibits three peaks, CO in the gas phase, CO bonding with PdO surface atoms, and CO adsorbed on the reduced metallic surface. (b) The 3d_{5/2} region from a 15 nm particle sample under the same conditions as in (a). The blue, yellow, and green components are identified with the same type of Pd atoms as in (a), whereas the purple component is attributed to the Pd atoms participating in the formation of a Pd-carbide. (c) Particle models displaying the origin of the different components in (b). To better illustrate the different types of Pd atoms, the particles have been made smaller than 15 nm.

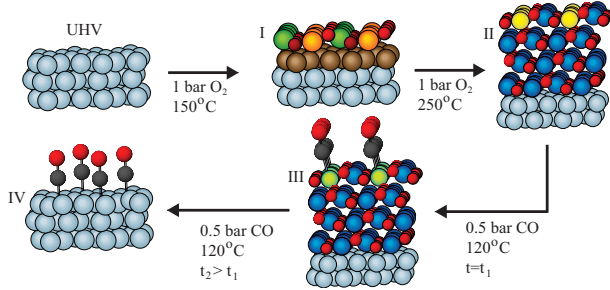


FIG. 6: Summary of the oxidation-reduction cycle of Pd(100). (I) As the crystal is heated in 1 mbar of O₂ the $\sqrt{5}$ surface oxide forms at a sample temperature of 150 °C. (II) Upon further heating the bulk oxide forms, and at T > 250 °C, the PdO film has grown thick enough to prevent detection of the metallic bulk in the Pd 3d_{5/2} level. (III) The reduction of the oxide takes place at sites on the oxide where CO can bind to Pd atoms coordinated to 2 O-atoms (green atoms). (IV) After the oxide is reduced, the Pd(100) surface is covered with CO adsorbed in bridge sites.

of 0.5 ML on Pd(100), CO is preferably adsorbed in a bridge configuration with an adsorption energy of 2.04 eV. On $\sqrt{5}$, the adsorption energy is 0.76 eV at 0.5 coverage (which corresponds to full coverage of the two-fold coordinated Pd atoms). The preferred configuration is in this case also bridge. On the 4 ML PdO(101) film,

CO adsorbs atop with a binding energy of 1.32 eV. The bridge site is in this case 0.1 eV higher in energy. This result is consistent with our calculation for adsorption on the bulk PdO(101) surface. CO is on this surface adsorbed by 1.35 eV when adopting an atop configuration and 1.24 eV in bridge. It should be noted that the site preference is coverage dependent. At 0.25 coverage, the two sites have the similar adsorption energies (~ 1.4 eV) on both PdO(101) and the 4ML system.

The results for the Pd(3d) SCLS in the presence of CO are collected in Table 2. The results are obtained with CO at 0.5 coverage (as defined above).

The Pd(3d) is shifted to higher binding energies in the presence of CO. For Pd(100) the shift is +0.46 eV when CO is adsorbed in bridge position. This is in good agreement with experimental results at the same coverage [49]. The Pd(3d) shift is even larger when CO is adsorbed atop. CO induces substantial shifts also for the $\sqrt{5}$ films. For the monolayer, the binding energy is shifted +1.6 eV with respect to Pd(3d) in the bulk when CO is adsorbed in bridge position. Adsorption atop yields a smaller shift. The reversed situation is predicted for the 4 ML case, where atop adsorption yields a larger shift than does bridge adsorption. The four-fold coordinated Pd atoms in the oxide films are only marginally affected by the CO adsorption.

The results we obtain for CO adsorption on bulk PdO(101) follows what we observed for the 4 ML surface oxide film on Pd(100). The Pd(3d) is shifted by

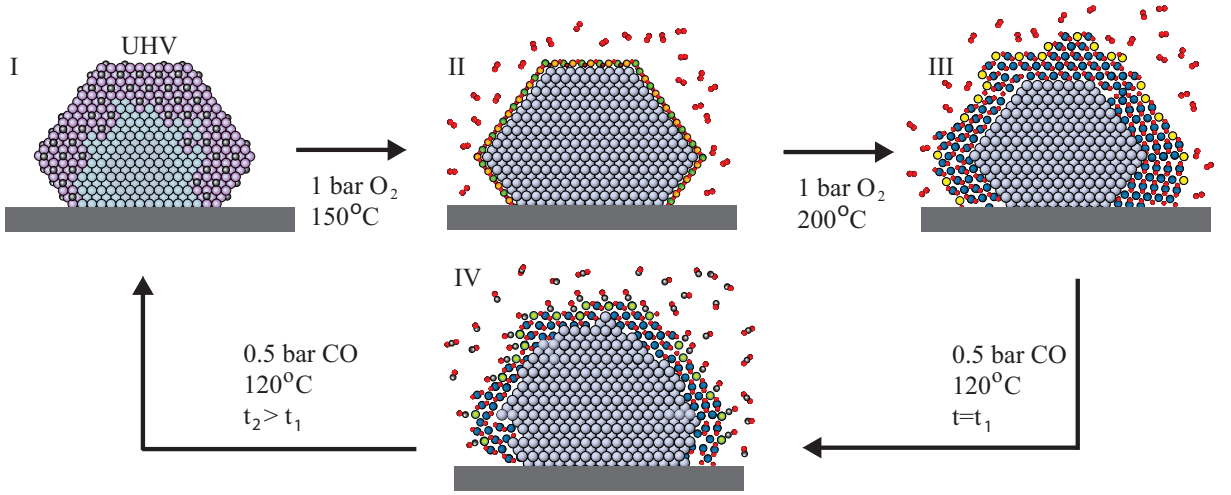


FIG. 7: Summary of the oxidation-reduction cycle of Pd nanoparticles ($15\text{nm} \leq \text{radius} \leq 35\text{ nm}$). (I) Starting with particles in a carbide phase. When the sample is heated in 1 mbar of O_2 the carbide is reduced, and as the sample temperature reaches 150° , our HPXPS data suggests that the particles are covered with a surface oxide (II). (III) Increasing the sample temperature 50° results in particles surrounded with a shell of PdO. (IV) When the O_2 atmosphere is replaced with 0.1 mbar of CO at 120° the oxide starts to decompose into metallic Pd and CO_2 . The reaction takes place at sites where CO can bind to 2-fold coordinated Pd atoms at the surface of the oxide (green atoms). When the oxide is reduced, we are again left in a carbide phase (I).

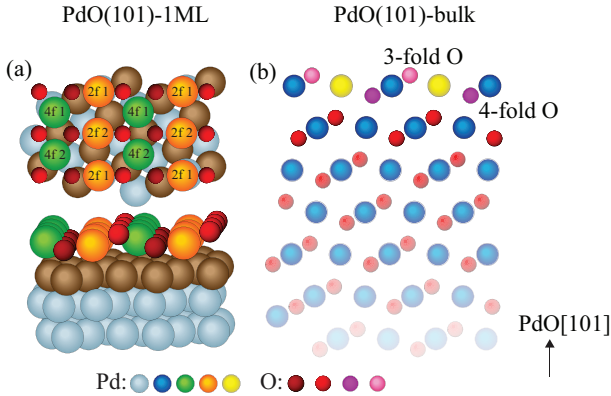


FIG. 8: Structural models considered in the calculations: (a) The $\sqrt{5}$ structure and (b) the PdO(101) surface. Four-fold and two-fold Pd atoms in the $\sqrt{5}$ structure are colored in green and orange, respectively. The first Pd(100) layer is colored in brown. For PdO(101), the two-fold and four-fold coordinated Pd atoms are colored in yellow and blue, whereas the three- and four-fold O-atoms are colored in pink and purple.

+0.80 eV (+0.35 eV) eV with respect to the a Pd atom in the bulk oxide when CO is adsorbed atop (bridge).

The $\sqrt{5}$ system with 4 ML of PdO(101) offers a way to evaluate the relative core level shifts of C(1s). For CO adsorbed in bridge at the PdO(101) film, the shift with respect to CO in bridge on Pd(100) is close to zero. Instead, when CO is adsorbed atop, the C(1s) binding energy is +1.14 eV.

TABLE II: Pd(3d) SCLS (eV) for CO adsorbed on Pd(100) and $\sqrt{5}$ with one and four monolayers. See Table 1 and Fig. 8 for description of the different Pd atoms.

	S0	2f ₁	2f ₂	4f ₁	4f ₂
bridge					
Pd(100) 0.46					
$\sqrt{5}$ 1ML	1.61	1.60	1.41	1.36	
$\sqrt{5}$ 4ML	1.48	1.48	1.20	1.17	
atop					
Pd(100) 0.93					
$\sqrt{5}$ 1ML	1.36	1.34	1.35	1.40	
$\sqrt{5}$ 4ML	1.95	1.95	1.20	1.20	

VI. DISCUSSION

A. Oxidation

First, it is important to note that all experimental oxidation studies of single crystal Pd samples at oxygen pressures above 1 mbar and temperatures at 300°C report growth of rough and disordered bulk PdO [53–57]. Previous experimental studies [53] using ex situ XPS combined with Low Energy Electron Diffraction [LEED] have shown that PdO grow on Pd(100) on the $\sqrt{5}$ in a Stranski-Krastanov growth mode at conditions similar to those used in the present investigations. The major difference from that study to ours is that we do not observe any metallic Pd for our PdO films. This shows that no $\sqrt{5}$ patches are present on the surface, demonstrating

the formation of a thicker PdO film. At higher temperatures and pressures, a thick and poorly ordered bulk PdO has also been observed [10, 54, 55]. In experiments the preferred surface orientation from bulk PdO has been found to be PdO(001)[56–58]. Although PdO(100) is predicted to be the most stable surface [41], thinner PdO films grown on the Pd(100) surface are stabilized in the PdO(101) direction [47]. This indicates the complexity of PdO growth on Pd(100).

In the present study we find surface components in the Pd 3d and O 1s core levels. The broad appearance of the components suggests that the PdO surface is indeed rough giving rise to a large number of peaks shifted with respect to each other by a small amount. This is consistent with the observation that also the oxidized Pd nanoparticles exhibit a very similar broadened bulk and surface emission. Obviously, the already random deposition of the particles will result in small PdO clusters randomly oriented on the SiO_x substrate.

For the initial oxidation of Pd(100) there is a good agreement between the experiments and the present calculations. The surface oxide has experimentally been formed at 150°C. This phase is characterized by two shifts in the Pd(3d) with respect to Pd in the bulk, namely 0.38 and, 1.3 eV. The average theoretical shifts are 0.40 and 1.19 eV, respectively. Upon further oxidation, the experimental intensity can be fitted to a good accuracy with two peaks centered at 1.3 and 1.6 eV. For the 4 ML $\sqrt{5}$ we calculate shifts of +0.53 and +1.14 eV. The calculations (which are in full agreement with previous reports [47]) yield similar Pd(3d) shifts for all Pd atoms that are four-fold coordinated, thus four-fold Pd atoms at the surface are masked by the bulk-contribution.

Although the experimental data and the calculations agree on two components for the oxidized Pd(100) surface the absolute shifts are in variance. One reason for the fairly large deviation could be that the oxidized surface is more complicated than simply continued PdO(101) growth. However, it is clear that the presence of (at least) one distinct surface component implies Pd atoms at the surface with reduced coordination. Another reason for the discrepancy could be the approximation to the exchange-correlation functional in the calculations. It is known that GGAs (such as PBE) fails to describe the experimentally observed band gap for PdO in the bulk [47].

Turning to a comparison of the oxidation rates of the Pd(100) single crystal and the Pd nanoparticles, our studies show that the particles form bulk PdO at lower temperatures than the single crystal. One reason for this behavior could be that the particles contains a larger number of defects such as steps, kinks and corners which are sites considered as beneficial for oxidation [59]. Indeed, lately it has been observed that one dimensional oxides may easily form at steps at UHV conditions containing under coordinated atoms on vicinal surfaces [60, 61]. In fact, it has been shown that the exact structure of the

1D oxide on the steps determines the rate of the continued growth of a 2D surface oxide [62]. A second reason could be the expected higher flexibility of a small nano particle as compared to a single crystal to accommodate oxygen atoms forming an oxide.

Recently, an in situ SXRD study of a sample containing Pd particles with gradually increasing size from 4 to 24 nm on MgO was performed [63, 64]. In that study, it was observed that when exposing 5 nm particles to 0.3 mbar of oxygen at 300°C bulk PdO was formed, although the bulk of the particles was still metallic. At 56 mbar and the same temperature, the 5 nm particles had oxidized completely, as evidenced by the complete disappearance of the Pd(111) reflection. Similar observations were done for the larger particles, apart from the fact that in the case of the larger particles, the Pd(111) reflection could always be observed, indicating that the bulk of the particles were not oxidized. These observations are consistent with the HPXPS observations reported here. We do not expect to probe deeper than a few PdO layers, and we observe very similar oxidation properties between the 15 and the 35 nm sized particles. Obviously, it would be interesting to study the oxidation of Pd nanoparticles with a very small size (< 3 nm). The reason is that it is not clear if the oxidation becomes easier or more difficult for very small particles, since on one hand the thermodynamic stability will decrease as the size of an oxide particle is decreasing, but on the other hand the bulk diffusion barriers is expected to decrease facilitating oxidation.

B. Reduction

During reduction, the presence of CO induces a marked shift of the Pd(3d) surface component on the oxidized systems. The calculated values for PdO(101) and the 4 ML $\sqrt{5}$ film are 0.35 (0.80) eV for CO in bridge (atop) configuration. Again, the agreement between the experiments and theory is only qualitative. Experimentally we find a shift of 0.55 eV in-between the calculated values. It is therefore likely that the CO induced component instead consists of two peaks which can not be resolved experimentally. We note that the match is much better for the partly reduced situation (the 1ML $\sqrt{5}$) and CO adsorbed on Pd(100).

The results for the C(1s) binding energies are clearer than for the Pd(3d). For CO adsorbed on the oxide, the C(1s) is measured to be shifted by ~ 1 eV on the oxide with respect to CO on Pd(100). The feature in the initial stage of the reduction is, however, broad and the possibility of two peaks with one at zero shift can not be ruled out. The calculations give a shifts of +1.1 eV for CO adsorbed atop on the oxide, whereas a zero shift is computed for CO at the bridge site. The presence of CO in the atop site conforms to the computed adsorption energies; CO is preferably adsorbed atop on the oxide and 4 ML $\sqrt{5}$ film.

The observation of CO adsorbing on the PdO surface indicate that under real conditions, CO could indeed adsorb on and react with oxygen in the PdO surface into CO₂ in a Mars-van Klevlen mechanism [10].

The observation of atomic carbon and the formation of Pd_xC by CO on oxide supported Pd particles have been observed previously, although the exact mechanism of the CO dissociation is still under debate [33, 67–70]. Our study confirms that a Pd_xC is exclusively formed on supported Pd particles [67–69] and is at variance with carbide formation on a Pd single crystal [71]. The present study does not reveal how the CO is dissociating, only that a Pd_xC is formed in the presence of CO. Nevertheless, it is clear that a full theoretical understanding of the CO oxidation over oxide supported Pd nanoparticles must include Pd_xC formation in a CO rich environment.

VII. CONCLUSIONS

To conclude, we have followed the oxidation by O₂ and reduction by CO of a Pd(100) single crystal as well as Pd nanoparticles supported on SiO_x substrates, using HPXPS. The oxidation and reduction behavior is similar for the nanoparticles and the single crystals with a surface oxide forming prior to the onset of the bulk oxidation. The temperature needed to start the formation of the bulk oxide is however lower on the particles as compared to the single crystal. We observe a core level shift for the under-coordinated Pd atoms at the surface

of the PdO oxide. This result is clearly illustrated by a change in the shift induced by adsorbed CO during the first stage of the reduction process. After the reduction, the single crystal was found in a metallic phase with CO adsorbed on the surface. In contrast, our results indicate that CO can dissociate on the nanoparticle model samples and form a Pd carbide. This is clearly different to the general belief that the active catalyst switches between an oxygen rich phase and a metallic phase where the catalyst is deactivated by adsorbed CO.

VIII. ACKNOWLEDGEMENT

This work was financially supported by the Swedish Research Council, the Crafoord foundation, the Knut and Alice Wallenberg foundation, the Foundation for strategic research (SSF) and the Anna and Edwin Berger foundation. This work was also supported by the Director, Office of Science, Office of Advanced Scientific Computing Research, Office of Basic Energy Sciences, Materials Sciences and Engineering, and Chemical Sciences, Geosciences, and Biosciences Division of the U.S. Department of Energy under Contract No. DE-AC02-05CH11231. The ESRF and ALS staff are gratefully acknowledged. The calculations were performed at C3SE (Göteborg).

IX. REFERENCES

-
- [1] E. Lundgren, A. Mikkelsen, J. N. Andersen, G. Kresse, M. Schmid, P. Varga, *J. Phys. Cond. Matter* **18** (2006) R481.
 - [2] M. Todorova, E. Lundgren, V. Blum, A. Mikkelsen, S. Gray, J. Gustafson, M. Borg, J. Rogal, K. Reuter, J. N. Andersen, M. Scheffler, *Surf. Sci.* **541** (2003) 101.
 - [3] P. Kostelnik, N. Seriani, G. Kresse, A. Mikkelsen, E. Lundgren, V. Blum, T. Sikola, P. Varga, M. Schmid, *Surf. Sci.* **601** (2007) 1574.
 - [4] E. Lundgren, G. Kresse, C. Klein, M. Borg, J. N. Andersen, M. De Santis, Y. Gauthier, C. Konvicka, M. Schmid, P. Varga, *Phys. Rev. Lett.* **88** (2002) 246103.
 - [5] H. Gabasch, W. Unterberger, K. Hayek, B. Klötzer, G. Kresse, C. Klein, M. Schmid, P. Varga, *Surf. Sci.* **600** (2006) 205.
 - [6] R. Westerström, C. J. Weststrate, A. Resta, A. Mikkelsen, J. Schnadt, J. N. Andersen, E. Lundgren, M. Schmid, N. Seriani, F. Mittendorfer, J. Harl, G. Kresse, *Surf. Sci.* **602** (2008) 2440.
 - [7] R. Westerström, C. J. Weststrate, J. Gustafson, A. Mikkelsen, J. Schnadt, J. N. Andersen, E. Lundgren, N. Seriani, F. Mittendorfer, G. Kresse, A. Stierle, *Phys. Rev. B* **80** (2009) 125431.
 - [8] B. L. M. Hendriksen and J. W. M. Frenken, *Phys. Rev. Lett.* **89** (2002) 046101.
 - [9] M.D. Ackermann, T. M. Pedersen, B.L.M. Hendriksen, O. Robach, S. C. Bobaru, I. Popa, C. Quiros, H. Kim, B. Hammer, S. Ferrer, J.W.M. Frenken, *Phys. Rev. Lett.* **95** (2005) 255505.
 - [10] B. L. M. Hendriksen, S. C. Bobaru, and J. W. M. Frenken, *Surf. Sci.* **552** (2004) 229.
 - [11] R. van Rijn, O. Balmes, R. Felici, J. Gustafsson, D. Wermeille, R. Westerström, E. Lundgren, J. W. M. Frenken, *J. Phys. Chem. C* **114** (2010) 6875.
 - [12] J. Gustafson, R. Westerström, A. Mikkelsen, X. Torrelles, O. Balmes, N. Bovet, J. N. Andersen, C. J. Baddeley, E. Lundgren, *Phys. Rev. B* **78** (2008) 045423.
 - [13] J. Gustafson, R. Westerström, A. Resta, A. Mikkelsen, J. N. Andersen, O. Balmes, X. Torrelles, M. Schmid, P. Varga, B. Hammer, G. Kresse, C. Baddeley, E. Lundgren, *Catalysis Today* **145** (2009) 227.
 - [14] J. Gustafson, R. Westerström, O. Balmes, A. Resta, R. van Rijn, X. Torrelles, C. T. Herbschleb, J. W. M. Frenken, E. Lundgren, *J. Phys. Chem. C* **114** (2010) 4580.
 - [15] H. Over, Y. D. Kim, A. P. Seitsonen, S. Wendt, E. Lundgren, M. Schmid, P. Varga, A. Morgante, and G. Ertl, *Science* **287** (2000) 1474.
 - [16] Y. B. He, M. Knapp, E. Lundgren, H. Over, *J. Phys. Chem. B* **109** (2005) 21825.
 - [17] H. Over, O. Balmes, E. Lundgren, *Catalysis Today* **145** (2009) 236.

- [18] R. Westerström, J. G. Wang, M. Ackermann, J. Gustafson, A. Resta, A. Mikkelsen, J. N. Andersen, E. Lundgren, O. Balmes, X. Torrelles, J. W. M. Frenken, B. Hammer, *J. Phys. Cond. Matter* **20** (2008) 184018.
- [19] J. Assmann, D. Crihan, M. Knapp, E. Lundgren, E. Löffler, M. Muhler, V. Narkhede, H. Over, M. Schmid, A. Seitsonen, P. Varga, *Angew. Chem. Int. Ed.* **44** (2005) 917.
- [20] P.-A. Carlsson, V. P. Zhdanov, M. Skoglundh, *Phys. Chem. Chem. Phys.* **8** (2006) 2703.
- [21] M. A. Newton, A. J. Dent, S. Diaz-Moreno, S. G. Fiddy, B. Jyoti, J. Evans, *Chem. Eur. J.*, **12** (2006) 1975.
- [22] M. E. Grass, Y. W. Zhang, D. R. Butcher, J. Y. Park, Y. M. Li, H. Bluhm, K. M. Bratlie, T. F. Zhang, G. A. Somorjai, *Angew. Chem. Int. Ed.* **47** (2008) 8893.
- [23] J. Rogal, K. Reuter, M. Scheffler, *Phys. Rev. Lett.* **98** (2007) 046101.
- [24] G. Rupprechter, C. Weilach, *Nano Today* **2** (2007) 20.
- [25] M. S. Chen, Y. Cai, Z. Yan, K. K. Gath, S. Axnanda, D. W. Goodman, *Surf. Sci.* **601** (2007) 5326.
- [26] Sh. Shaikhutdinov, M. Heemeier, J. Hoffmann, I. Meusel, B. Richter, M. Bumer, H. Kuhlenbeck, J. Libuda, H. -J. Freund, R. Oldman, S. D. Jackson, C. Konvicka, M. Schmid, P. Varga, *Surf. Sci.* **501** (2002) 270.
- [27] T. Schalow, B. Brandt, D. E. Starr, M. Laurin, S. K. Shaikhutdinov, S. Schauermaun, J. Libuda, H.-J. Freund, *Angew. Chem. Int. Ed.* **45** (2006) 3693.
- [28] T. Schalow, M. Laurin, B. Brandt, S. Schauermaun, S. Guimond, H. Kuhlenbeck, D. E. Starr, S. K. Shaikhutdinov, J. Libuda, H.-J. Freund, *Angew. Chem. Int. Ed.* **44**, (2005) 7601.
- [29] T. Schalow, B. Brandt, M. Laurin, S. Schauermaun, S. Guimond, H. Kuhlenbeck, J. Libuda, H.-J. Freund *Surf. Sci.* **600**, 2528 (2006).
- [30] H.J. Ruppender, M. Grunze, C.W. Kong, M. Wilmers, *Surf. Interface Anal.* **15** (1990) 245.
- [31] H. Bluhm, M. Hävecker, A. Knop-Gericke, E. Kleimenov, R. Schlögl, D. Teschner, V.I. Bukhtiyarov, D.F. Ogletree, M. Salmeron, *J. Phys. Chem. B* **108**, 14340 (2004).
- [32] M. E. Messing, K. A. Dick, L. R. Wallenberg, K. Deppert, *Gold Bull.* **42** (2009) 20.
- [33] M. A. Newton, M. Di Michiel, A. Kubacka, M. Fernandez-Garcia, *J. Am. Chem. Soc.* **132** 4540 (2010)
- [34] M. E. Messing, R. Westerström, B. O. Meuller, S. Blomberg, J. Gustafson, J. N. Andersen, E. Lundgren, R. van Rijn, O. Balmes, H. Bluhm and K. Deppert *J. Phys. Chem. C.* **114**, 9257 (2010).
- [35] R. Nyholm, M. Qvarford, J. N. Andersen, S. L. Sorensen and C. Wigren, *J. Phys. Condens. Matter* **4** (1992) 277.
- [36] S. J. Clark, M. D. Segall, C. J. Pickard, P. J. Hasnip, M. J. Probert, K. Refson, and M. C. Payne, *Zeitschrift fuer Kristallographie* **220**, 567 (2005).
- [37] note We use the CASTEP program.
- [38] J. P. Perdew, K. Burke, and M. Ernzerhof, *Phys. Rev. Lett.* **77**, 3865 (1996).
- [39] D. Vanderbilt, *Phys. Rev. B* **41**, 7892 (1990).
- [40] D. R. Lide, ed., *Handbook of Chemistry and Physics* (publisher CRC Press, Inc., 2009-2010), 90th ed.
- [41] J. Rogal, K. Reuter, and M. Scheffler, *Phys. Rev. B* **69**, 075421 (2004).
- [42] E. Pehlke and M. Scheffler, *Phys. Rev. Lett.* **71**, 2338 (1993).
- [43] H. Bluhm, M. Hävecker, A. Knopp-Gericke, M. Kiskinova, R. Schlögl, M. Salmeron, *MRS Bulletin* **32** (2007) 1010.
- [44] D. Zemlyanov, B. Aszalos-Kiss, E. Kleimenov, D. Teschner, S. Zafeiratos, M. Hävecker, A. Knop-Gericke, R. Schlögl, H. Gabasch, W. Unterberger, K Hayek, Bernhard Klötzer, *Surf. Sci.* **600** (2006) 983.
- [45] H. Gabasch, W. Unterberger, K. Hayek, B. Klötzer, E. Kleimenov, D. Teschner, S. Zafeiratos, M. Hävecker, A. Knop-Gericke, R. Schlögl, J. Han, F. H. Ribeiro, B. Aszalos-Kiss, T. Curtin, D. Zemlyanov, *Surf. Sci.* **600** (2006) 2980.
- [46] G. Ketteler, D.F. Ogletree, H. Bluhm, H. Liu, E.L.D. Hebenstreit, M. Salmeron, *J. Am. Chem. Soc.* **127** (2005) 18269.
- [47] N. Seriani, J. Harl, F. Mittendorfer, G. Kresse *J. Chem. Phys.* **131** (2009) 054701.
- [48] R. Westerström, J. Gustafson, A. Resta, A. Mikkelsen, J.N. Andersen, E. Lundgren, N. Seriani, F. Mittendorfer, M. Schmid, J. Klimovits, P. Varga, M. D. Ackermann, J.W.M. Frenken, N. Kasper, A. Stierle, *Phys. Rev. B* **76** (2007) 155410.
- [49] J. N. Andersen, M. Qvarford, R. Nyholm, S. L. Sorensen, C. Wigren, *Phys. Rev. Lett.* **67** (1991) 2822.
- [50] N. Seriani, F. Mittendorf, G. Kresse, *J. Phys. Chem.* **132** (2010) 024711.
- [51] J. Rogal, K. Reuter, and M. Scheffler, *Phys. Rev. Lett.* **98**, 046101 (2007).
- [52] J. Rogal, K. Reuter, and M. Scheffler, *Phys. Rev. B* **75**, 205433 (2007).
- [53] J. Wang, Y. Yun, E. I. Altman, *Surf. Sci.* **601** (2007) 3497.
- [54] J. Han, D. Y. Zemlyanov, F. H. Ribeiro, *Surf. Sci.* **600** (2006) 2730.
- [55] J. Han, D. Y. Zemlyanov, F. H. Ribeiro, *Surf. Sci.* **600** (2006) 2752.
- [56] E. Lundgren, J. Gustafson, A. Mikkelsen, J. N. Andersen, A. Stierle, H. Dosch, M. Todorova, J. Rogal, K. Reuter, M. Scheffler, *Phys. Rev. Lett.* **92** 046101 (2004).
- [57] A. Stierle, N. Kasper, H. Dosch, E. Lundgren, J. Gustafson, A. Mikkelsen, J. N. Andersen, *J. Chem. Phys.* **122** 044706 (2005).
- [58] J. R. McBride, K. C. Hass, W. H. Weber, *Phys. Rev. B* **44** (1991) 5016.
- [59] K. Reuter, C. Stampfl, M. V. Ganduglia-Pirovano, M. Scheffler, *Chem. Phys. Lett.* **352** (2002) 311.
- [60] J. G. Wang, W. X. Li, M. Borg, J. Gustafson, A. Mikkelsen, T. M. Pedersen, E. Lundgren, J. Weissenrieder, J. Klimovits, M. Schmid, B. Hammer, and J. N. Andersen, *Phys. Rev. Lett.* **95** (2005) 256102 .
- [61] J. Gustafson, A. Resta, A. Mikkelsen, R. Westerström, J. N. Andersen, E. Lundgren, J. Weissenrieder, M. Schmid, P. Varga, N. Kasper, X. Torrelles, S. Ferrer, F. Mittendorfer, G. Kresse, *Phys. Rev. B* **74** (2006) 035401.
- [62] J. Klimovits, M. Schmid, L. R. Merte, P. Varga, R. Westerström, A. Resta, J. N. Andersen, J. Gustafson, A. Mikkelsen, E. Lundgren, F. Mittendorfer and G. Kresse, *Phys. Rev. Lett.* **101** (2008) 266104.
- [63] P. Nolte, A. Stierle, N. Kasper, N. Y. Jin-Phillipp, H. Reichert, A. Rühm, J. Okasinski, H. Dosch, S. Schöder, *Phys. Rev. B* **77** (2008) 115444.
- [64] A. Stierle, *Int. J. Mat. Res.* **100** (2009) 10.
- [65] E. Lundgren, J. N. Andersen, Unpublished.
- [66] J. Rogal, *Stability, Composition and Function of Palladium Surfaces in Oxidizing Environments: A First-*

- Principles Statistical Mechanics Approach*, (Ph.D thesis, Fritz Haber Institute of the Max Planck Society Theory Department, 2006).
- [67] G. Rupprechter, V. V. Kaichev, H. Unterhalt, M. Morkela, V. I. Bukhti, Appl. Surf. Sci. **235** (2004) 26.
 - [68] V. V. Kaicheva, M. Morkel, H. Unterhalt, I. P. Prosvirin, V. I. Bukhtiyarov, G. Rupprechter, and H. -J. Freund, Surf. Sci. **566** (2004) 1024
 - [69] K. Föttinger, R. Schlögl and G. Rupprechter, Chem. Commun., **3** (2008), 320.
 - [70] E. Ozensoy, B. K. Min, A. K. Santra, and D. W. Goodman J. Phys. Chem. B **108** (2004) 4351.
 - [71] V. Matolin, M. Rebholz, N. Kruse Surf. Sci. **245** (1991) 233.